B-T-3462

Transmission electron microscopy of oxide dispersion strengthened (ODS) molybdenum: effects of irradiation on material microstructure

R. Baranwal, and M. G. Burke

NOTICE

BECHTEL BETTIS, INC. WEST MIFFLIN, PENNSYLVANIA 15122-0079

Transmission electron microscopy of oxide dispersion strengthened (ODS) molybdenum: effects of irradiation on material microstructure

R. Baranwal and M. G. Burke

Bechtel Bettis, Inc., P. O. Box 79, West Mifflin, PA 15122-0079

ABSTRACT

Oxide dispersion strengthened (ODS) molybdenum has been characterized using transmission electron microscopy (TEM) to determine the effects of irradiation on material microstructure. This work describes the results-to-date from TEM characterization of unirradiated and irradiated ODS molybdenum. The general microstructure of the unirradiated material consists of fine molybdenum grains (< 5 μm average grain size) with numerous low angle boundaries and isolated dislocation networks. 'Ribbon'-like lanthanum oxides are aligned along the working direction of the product form and are frequently associated with grain boundaries, serving to inhibit grain boundary and dislocation movement. In addition to the 'ribbons', discrete lanthanum oxide particles have also been detected. After irradiation, the material is characterized by the presence of non-uniformly distributed large (~ 20 to 100 nm in diameter), multi-faceted voids, while the molybdenum grain size and oxide morphology appear to be unaffected by irradiation.

§1. INTRODUCTION

Oxide Dispersion Strengthened (ODS) molybdenum is attractive for high-temperature applications due to its excellent high-temperature mechanical properties (Mueller *et al.* 2000). It is believed that the dispersed oxide phase in the alloy improves creep resistance by impeding grain boundary sliding and dislocation motion compared to the behavior of unalloyed molybdenum. To optimize the mechanical behavior of these materials, it is necessary to characterize and understand the microstructure in terms of grain size, substructure, and second phase particles, and, in turn, understand how the microstructure affects material behavior. The structure and properties of molybdenum have been well documented, particularly the response of unalloyed molybdenum and molybdenum alloys to neutron irradiation (Abe *et al.* 1993, Adda 1972, Bentley 1974, Brimhall *et al.* 1973,

Evans 1980, Eyre 1972, Gelles *et al.* 1981, Sikka and Moteff 1974, Tewary and Bullough 1972). Typical irradiation-induced defects that can form in the microstructure include cavities or voids, 'black spots' (clusters of points defects), dislocations, and dislocation loops. The frequency, distribution, and size of these defects will depend upon the irradiation temperature and fluence. To determine whether ODS molybdenum exhibits similar behavior as unalloyed molybdenum, ODS molybdenum specimens were irradiated at ~1000°C in order to characterize the effect of neutron irradiation on the microstructure.

This work describes the results from characterization of ODS molybdenum, where the oxide is lanthanum (La) oxide, and compares unirradiated ODS molybdenum samples with irradiated specimens to provide data on the effects of irradiation on material microstructure. The microstructure of these materials has been characterized using a variety of sophisticated methods, including focused ion beam (FIB) techniques and transmission electron microscopy (TEM).

§2. EXPERIMENTAL

The material studied in this investigation was produced per U.S. patent 5 868 876 and a proprietary powder metallurgy procedure. The process results in a ~0.75 mm thick ODS molybdenum sheet containing a nominal two-volume percent lanthanum oxide. The original sheet material was evaluated in the stress-relieved (typically 1 h at 1200 °C) condition. To assess the microstructure of the as-received ODS-molybdenum sheet, bulk sections from the short-transverse and longitudinal-transverse orientations were examined using the secondary electron imaging capability of a focused ion beam (FIB) instrument. After FIB micromachining to remove the as-cut surfaces, secondary electron images were acquired using the primary Ga^+ ion beam. A Micron 2500 Focused Ion Beam instrument with a 50 kV Ga^+ beam was used for general metallographic characterization. The enhanced channeling contrast enabled the polycrystalline structure to be readily assessed.

Further detailed microstructural characterization of the as-received material was performed using Transmission Electron Microscopy. Plan-view TEM specimens were electropolished in a 13 % H_2SO_4 – 87 % CH_3OH solution at 0 °C and 20 volts using a Struers Tenupol. Electron-transparent specimens were examined in Philips

CM12 and a CM300 Field Emission Gun (FEG) Analytical Transmission Electron Microscopes operated at 120 kV and 300 kV, respectively. The Philips CM300 FEG ATEM was equipped with an Oxford ISIS 300 energy dispersive x-ray spectrometer (EDS) and analysis system.

Specimens (3 mm-diameter, 0.25 mm-thick discs) were also irradiated in the High Flux Isotope Reactor (HFIR) at Oak Ridge National Laboratory (ORNL) at ~1000°C to fluences of ~2 x 10^{21} n cm^{-2} (1.2 dpa) and ~6 x 10^{21} n cm^{-2} (3.40 dpa) (E > 0.1 MeV) at a fast neutron flux of 8.5 x 10^{14} n cm^{-2}-sec. Electron-transparent samples for TEM characterization were prepared in the same manner as the unirradiated materials. These thin-foil specimens were subsequently examined in a Philips EM420 Analytical Transmission Electron Microscope operated at 120 kV.

§3. RESULTS

§3.1 Characterization of unirradiated ODS molybdenum sheet

The general microstructure of the unirradiated was evaluated using the secondary electron imaging mode of the FIB. The FIB secondary electron images of the longitudinal-transverse and short-transverse sections, shown in Figures 1 and 2, respectively, revealed a very fine-grained molybdenum microstructure, with pancaked (elongated) grains aligned in the rolling direction. The molybdenum grains extended up to ~10 μm in length, with thicknesses of ~1-2 μm. Throughout the microstructure, a brightly-imaging elongated phase was observed, primarily at grain boundaries. These second phase 'ribbons' extended up to ~30 μm in length. The secondary electron image in Figure 2 also shows the oxide 'ribbons' in cross-section as well as the discrete brightly-imaging oxide particles.

{Insert figures 1 and 2 about here}

More detailed characterization was performed via TEM analysis. The general microstructure of these unirradiated materials consisted of fine molybdenum grains with numerous low angle boundaries and dislocation networks. Figure 3 contains a bright-field transmission electron microscopy (TEM) image showing the microstructure of the ODS molybdenum in plan-view (parallel to the rolling plane). Numerous subgrains and isolated dislocation networks are evident. These specimens were characterized by the presence of both

intra- and intergranular oxides, though the intergranular oxides were more prevalent. The intergranular oxide 'ribbons' were ~100 nm thick, 200-500 nm wide, and up to 30 microns long. These oxide 'ribbons' are frequently associated with grain boundaries, are aligned along the working direction of the product form, as depicted in the schematic diagram of Figure 4, and serve to inhibit grain boundary movement. In addition to the 'ribbons', discrete lanthanum oxide particles have also been detected both within the grains and at grain boundaries. The discrete intragranular particles appeared as ~30 to 200 nm spheroids. TEM analysis of the plan-view specimens also revealed that the spheroidal oxides were aligned along the working direction.

{Insert figures 3 and 4 about here}

The development of the 'ribbon'-like lanthanum oxides during thermomechanical processing of the material coupled with presence of numerous dislocations and fine subgrains within the electron-transparent 'ribbons' (as observed by TEM)[RB1] suggest that the lanthanum oxides may be deformable, possibly due to small amounts (< 5 wt.%) of molybdenum (detected by STEM-EDS microanalysis) in some oxides. Furthermore, it is speculated that the metal-'ribbon' interface may be essential to the high-temperature mechanical properties of these alloys. It is important to note that although electron diffraction of selected oxides confirmed that those analyzed oxide particles were La_2O_3, not all oxides present in the ODS molybdenum specimens may be pure La_2O_3.

§3.2 Characterization of irradiated ODS molybdenum sheet

§3.2.1: ODS molybdenum irradiated to a fluence of 2.3 x 10^{21} n cm^{-2} (~1000°C): This material was characterized by the presence of large, multi-faceted voids, predominantly hexadodecahedral-shaped and nonuniformly distributed within the matrix (Figures 5-7). The voids ranged in size from ~20 nm to a maximum of ~100 nm. The average void diameter for this material determined via image analysis is ~50 nm, and a local maximum void density was estimated to be ~1 x 10^{14} voids cm^{-3}. When viewed on the (111) plane, the voids appear to be hexagonal and when viewed on the (100) plane, they appear square (Figure 5). Therefore, the overall shape of the voids may actually be hexadodecahedral, six square faces and 12 hexagonal faces.

{Insert figure 5 about here}

It should be noted that voids that intersected the foil surfaces were not measured because these voids may become enlarged by the electrolyte, leading to the artifact of apparently coarser voids. The voids that intersect

the foil surfaces can also be identified by the change in void morphology caused by exposure to the electrolyte; the voids that form in molybdenum are facetted, hexadodecahedrally-shaped voids while the voids that intersect the foil surfaces become rounded or oval.

The voids also appeared to be aligned with respect to the working direction of the sheet in these plan-view foils (Figure 6). Some of the voids were associated with isolated lanthanum oxide particles. Isolated dislocations were occasionally observed in association with some voids, including some dislocations pinned by voids (Figure 7). The original microstructure of the specimen (molybdenum grain size and morphology of lanthanum oxide ribbons) appears to be unaffected by neutron irradiation (Figure 6). This is not unexpected because the irradiation temperature of ~1000°C is well below the one-hour recrystallization temperature (1700°C) of this material. Furthermore, the stress relief heat treatment of the material can decrease the driving force for recrystallization and grain growth, and may also provide resistance to irradiation damage up to high fluences, as has been reported by Abe *et al*, 1993.

{Insert figures 6 and 7 about here}

Defects such as dislocation loops and 'black spot' damage were not observed in the analyzed areas of the ODS molybdenum TEM foils irradiated at ~1000°C, consistent with expectations for materials irradiated at such high temperatures (Bentley 1974 and Sikka and Moteff 1974).

3.2.2: ODS molybdenum irradiated to a fluence of 6.4 x 10^{21} n cm^{-2} (~1000°C): A significant increase in the proportion of voids relative to the low fluence irradiated material was observed during TEM examination of this material (Figures 8-10). The void morphology remained facetted, as in the lower fluence material; however, the voids appeared to be more uniformly distributed than those detected in the lower fluence material. The coarser voids still appeared to be aligned with the working direction of the sheet.

{Insert figures 8, 9a, and 9b about here}

A narrow 'void-free zone' was observed adjacent to grain boundaries (Figure 10). The very fine-grained structure of the material was similar to that observed in the lower fluence samples. The average void diameter

for this material measured via image analysis was 30 nm, with a size range of ~10 to ~100 nm, with an estimated local maximum void density of ~1.7 x 10^{15} voids cm^{-3} .

{Insert figure 10 about here}

Similar to the lower fluence samples, the original microstructure of the specimen (molybdenum grain size and morphology of lanthanum oxide ribbons) after irradiation to 6.4 x 10^{21} n cm^{-2} appeared to be unaffected by neutron irradiation (Figure 8). Also, like the material irradiated to 2.3 x 10^{21} n cm^{-2}, no evidence of dislocation loops and 'black spot' damage was observed.

§4. DISCUSSION

The TEM data for these ODS molybdenum specimens showed that the average void size decreased with increasing fluence, which is in agreement with other TEM data for irradiated molybdenum (Bentley 1974). This decrease in average void size was accompanied by an increase in void number density, which also is consistent with other experimental and theoretical work (Eyre 1972, Tewary and Bullough 1972). One possible explanation for the apparent 'shrinkage' of voids as fluence increases may be related to the start of the formation of a void lattice (Bentley 1974). Another explanation for the apparent shrinkage of voids with increasing fluence may be related to the presence of the lanthanum oxide particles. The lower fluence ODS molybdenum specimens were characterized by a non-random distribution of rather coarse voids. This suggests that void nucleation may initially occur at preferential sites, such as the incoherent lanthanum oxide particles within the microstructure. As the fluence increases and the heterogeneous void nucleation associated with the lanthanum oxide particles becomes saturated, more vacancies are produced and new, smaller voids can homogeneously nucleate (Bloom 1972), resulting in an increased proportion of finer voids in the ODS molybdenum. The newly formed fine voids shift the average size to lower values in the resulting void size distribution but increase the void number density as observed by TEM. Another reason for the apparent shrinkage of voids with an increase in irradiation fluence may be due to the migration of transmutation impurities (e.g. technetium, ruthenium, cerium) to the void surface that, upon accumulation, prevent the flow of additional vacancies into the already existing voids (Evans 1980). If vacancy motion to existing voids is restricted, local vacancy concentration will rise, resulting in nucleation of new voids, as is seen in the current work.

The very fine molybdenum grain structure that characterizes the ODS molybdenum materials provides a high proportion of sinks, such as grain boundaries and dislocation networks, as well as the incoherent oxide/metal interfaces. It is possible that the vacancies in the vicinity of these sinks will annihilate at these sinks (Figure 10), and that the remaining vacancies coalesce to form the observed voids (particularly those near the center of the very fine grains). The voids in the irradiated ODS molybdenum material appeared to be aligned along the working direction of the sheet. The observations reported herein suggest that the material anisotropy and lanthanum oxide particles may be affecting the size and distribution of the voids, as heterogeneous nucleation of voids on second phase particles has been previously reported (Bloom 1972).

The size and shape of the voids seen in ODS molybdenum irradiated to a fluence of ~2 x 10^{21} n cm^{-2} (1000 °C) are consistent with what has been reported in the literature for pure molybdenum. Molybdenum samples irradiated at 1200°C to 5 x 10^{20} n cm^{-2} had 30 – 60 nm voids, a void density of 10^{14} cm^{-3}, and volumetric swelling ($\Delta V/V_o$) of 0.2% (Adda 1972). Molybdenum samples irradiated at 900°C to 5 x 10^{20} n cm^{-2} had 8 – 20 nm voids, a void density of 3x10^{15} cm^{-3}, and swelling ($\Delta V/V_o$) of 0.2-0.4 % (Adda 1972). Molybdenum samples irradiated at 985°C to 1 x 10^{21} n cm^{-2} had a mean void diameter of 26 nm, a void density of 3.5 x 10^{14} cm^{-3}, and swelling ($\Delta V/V_o$) of 0.47% (Brimhall *et al.* 1973). The dodecahedral shape of the voids has been reported for molybdenum irradiated at 850°C to 1 x 10^{20} n cm^{-2} (Bentley 1974) and at 985°C to 1 x 10^{21} n cm^{-2} (Brimhall *et al.* 1973).

Local maximum swelling in the ODS molybdenum material, determined from TEM measurements, is consistent with literature data. The swelling for the ODS molybdenum material was estimated to be less than ~1 % for the low fluence material and less than ~2.4 % for the material irradiated to a fluence of ~6 x 10^{21} n cm^{-2}. Literature data have indicated that the irradiation swelling of molybdenum is very low (Brimhall *et al.* 1973, Gelles *et al.* 1981, Abe *et al.* 1993, Evans 1980). Volumetric swelling of 0.12 % has been reported for unalloyed molybdenum irradiated to 970 °C to a fluence of 1.96 x 10^{21} n cm^{-2} (Brimhall *et al.*, 1973). A maximum volumetric swelling of 1.6% has been reported for unalloyed molybdenum irradiated to 600 °C to a neutron fluence of 9.6 x 10^{22} n cm^{-2} (E > 0.1 MeV)(Abe *et al.* 1973). Additionally, a maximum volumetric swelling of

3.3% has been reported for TZM molybdenum irradiated at 650 °C to a fluence of 1.76 x 10^{23} n cm^{-2} (E > 0.1 MeV) (Gelles *et al.* 1981).

§5. SUMMARY

TEM analyses of ODS molybdenum samples irradiated at ~1000°C revealed the presence of facetted voids, the size range of which varied from 5 to <100 nm, depending upon fluence. ODS molybdenum irradiated to a fluence of ~2 x 10^{21} n cm^{-2} had an average void diameter of ~50 nm. The local maximum swelling was estimated to be less than ~1%. After irradiation to a fluence of ~6 x 10^{21} n cm^{-2}, the average void diameter was ~30 nm. The local maximum swelling for this material was estimated to be less than ~2.4%.

The observations of void formation in the irradiated ODS molybdenum samples are consistent with literature data for unalloyed molybdenum and other molybdenum alloys. Similarly, TEM data indicate that void swelling in these materials is low.

ACKNOWLEDGEMENTS

The authors thank M. W. Phaneuf of Fibics, Inc. for FIB micromachining and imaging, A. J. Falco and R. T. Pieretti for TEM foil preparation, and D. L. Ward for image analysis.

REFERENCES

Abe, K., Masuyama, T., Satou, M., and Hamilton, M. L., 1993, *Mat. Trans. JIM,* **34,** 1137.

Adda, Y., 1972, *Radiation-Induced Voids in Metals,* Proceedings of the 1971 International Conference, edited by J. W. Corbett and L. C. Ianniello (Oak Ridge, TN: U.S. Atomic Energy Commission), pp. 31-83.

Bentley, J., 1974, PhD Thesis, Univ. of Birmingham, UK.

Bloom, E. E., 1972, *Radiation-Induced Voids in Metals*, Proceedings of the 1971 International Conference, edited by J. W. Corbett and L. C. Ianniello (Oak Ridge, TN: U.S. Atomic Energy Commission), pp. 1-30.

Brimhall, J. L., Simonen, E. P., and Kissinger, H. E., 1973, *J. Nucl. Mater.*, **48,** 339.

Evans, J. H., 1980, *J. Nucl. Mater.*, **88,** 31.

Eyre, B. L., 1972, *Defects in Refractory Metals*, Proceedings of the International Discussion Meeting, edited by R. de Batist, J. Nihoul, and L. Stals (Mol, Belgium: SCK/CEN), pp. 311-350.

Gelles, D. S., Peterson, D. T., and Bates, J. F., 1981, *J. Nucl. Mater.*, **103 & 104,** 1141.

Mueller, A.J., Bianco, R., and Buckman, R.W., 2000, *Int'l Journal of Refractory Metals & Hard Materials*, **18,** 205.

Sikka, V. K. and Moteff, J., 1974, *Nuc. Tech.*, **22,** 52.

Tewary, V. K. and Bullough, R., 1972, *J. Phys. F. (Metal Phys.),* **2,** L69.

FIGURE CAPTIONS

Figure 1. FIB secondary electron image of the longitudinal-transverse section showing the grain structure and brightly-imaging lanthanum oxide 'ribbons' (arrowed) and discrete oxide particles aligned along the rolling direction in the mid-thickness region of a 0.75 mm-thick sheet sample (field of view = 20μm).

Figure 2. FIB secondary electron image of the short-transverse section showing the grain structure and brightly-imaging lanthanum oxide 'ribbons' (arrowed) and discrete oxide particles in the mid-thickness region of a 0.75 mm-thick sheet sample (field of view = 20μm). The rolling direction is normal to the image plane.

Figure 3. TEM image of the ODS molybdenum sheet (plan view) showing the presence of discrete and 'ribbon' oxides (labelled), isolated dislocations, dislocation networks and grain boundaries.

Figure 4: Schematic diagram showing the various oxide morphologies (black features in the diagram) in the 0.75 mm-thick ODS molybdenum sheet. TEM foils from the sheet material were prepared parallel to the rolling plane (plan-view). In the ODS molybdenum sheet specimens, 'ribbon'-like oxides are aligned with the rolling direction.

Figure 5. TEM image of ODS molybdenum irradiated to ~2 x 10^{21}n cm^{-2} at ~1000°C showing the presence of facetted, hexadodecahedral-shaped voids within the metal.

Figure 6. TEM image of ODS molybdenum irradiated to ~2 x 10^{21} n cm^{-2} at ~1000°C. Note the presence of lanthanum oxide "ribbons" and discrete darkly-imaging lanthanum oxide particles (white arrows) within the microstructure. The irradiation-induced voids appear to be aligned (black arrows) along working direction of the sheet. The grain size and lanthanum oxide morphologies appeared to be unaffected by neutron irradiation.

Figure 7. TEM image of ODS molybdenum irradiated to ~2 x 10^{21} n cm^{-2} at ~1000°C. Note the aligned voids and the voids associated with the discrete lanthanum oxide particle within the matrix. Evidence of dislocation pinning by the voids is observed (arrowed).

Figure 8. TEM image of ODS molybdenum irradiated to ~6 x 10^{21} n cm^{-2} at ~1000°C. The grain size and lanthanum oxide morphologies appeared to be unaffected by neutron irradiation. Note the more uniform distribution of voids.

Figure 9. (a, b) TEM images of ODS molybdenum irradiated to ~6 x 10^{21} n cm^{-2} at ~1000°C. Note the hexadodecahedrally facetted voids in (b).

Figure 10. TEM image of ODS molybdenum irradiated to ~6 x 10^{21} n cm^{-2} at ~1000°C. Note the narrow void-free zone adjacent to the grain boundaries, which act as local sinks for vacancies.

\

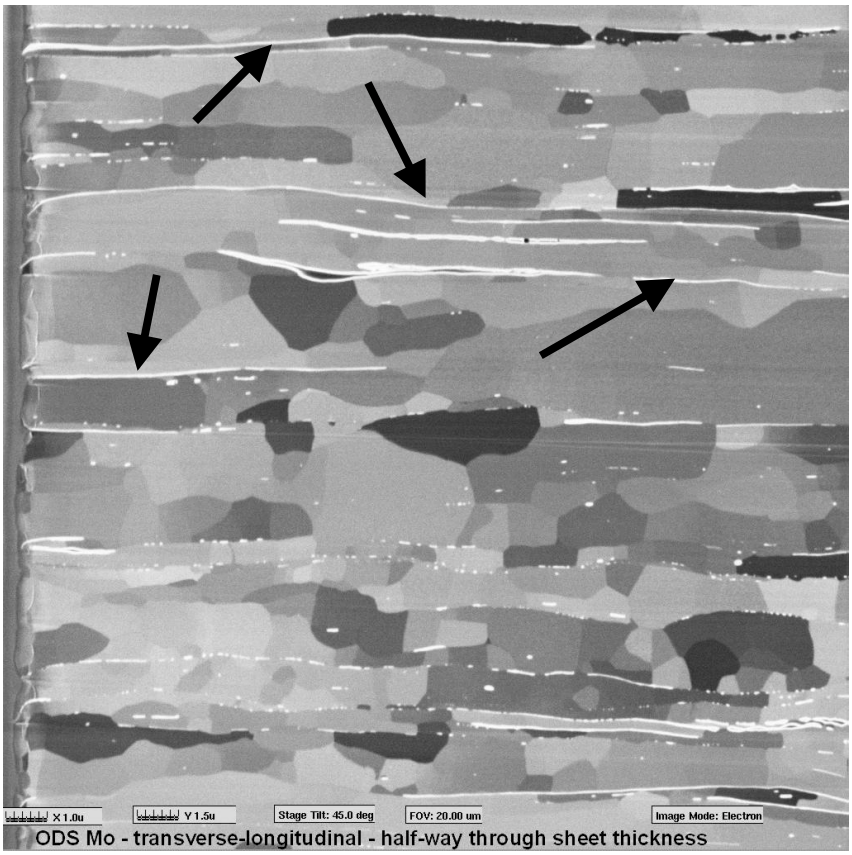
X 1.0u
Y 1.5u
Stage Tilt: 45.0 deg
FOV: 20.00 um
Image Mode: Electron
ODS Mo - transverse-longitudinal - half-way through sheet thickness

Figure 1.

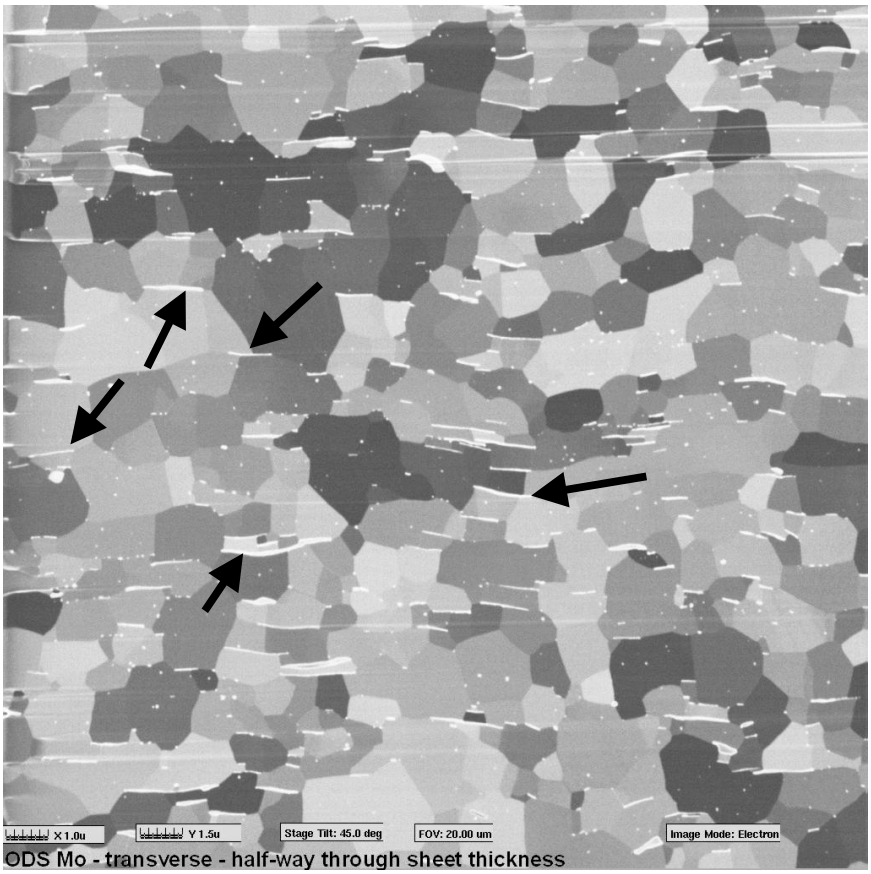
X 1.0u
Y 1.5u
Stage Tilt: 45.0 deg
FOV: 20.00 um
Image Mode: Electron
ODS Mo - transverse - half-way through sheet thickness

Figure 2.

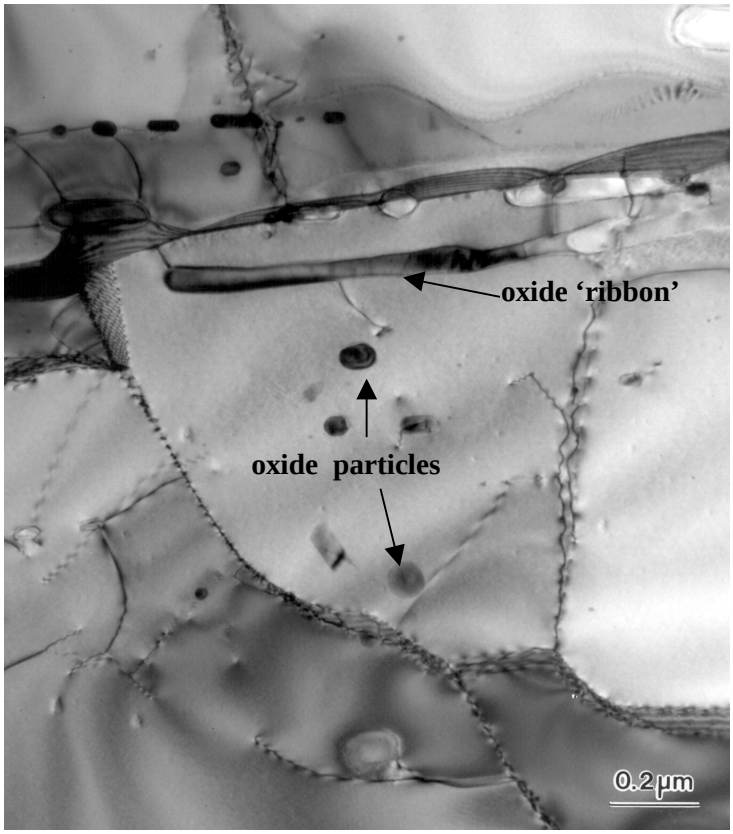

Figure 3.

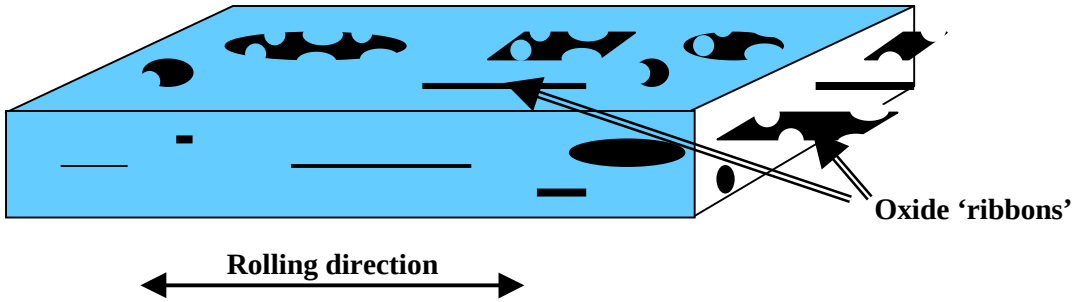

Figure 4.

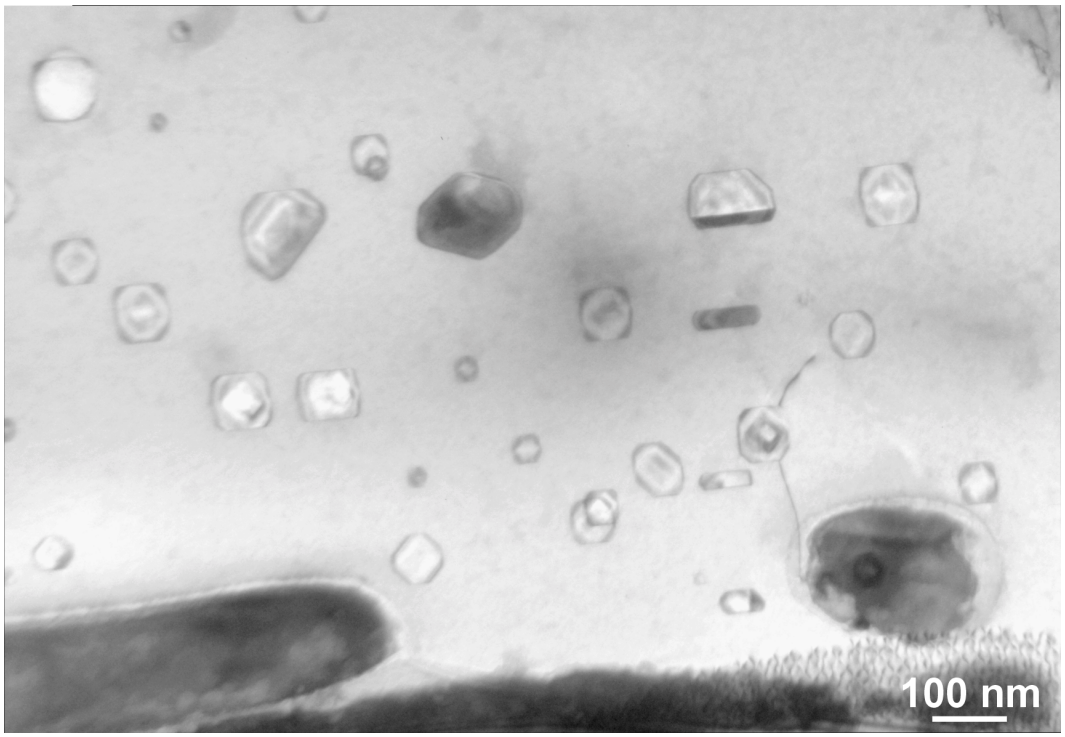

Figure 5.

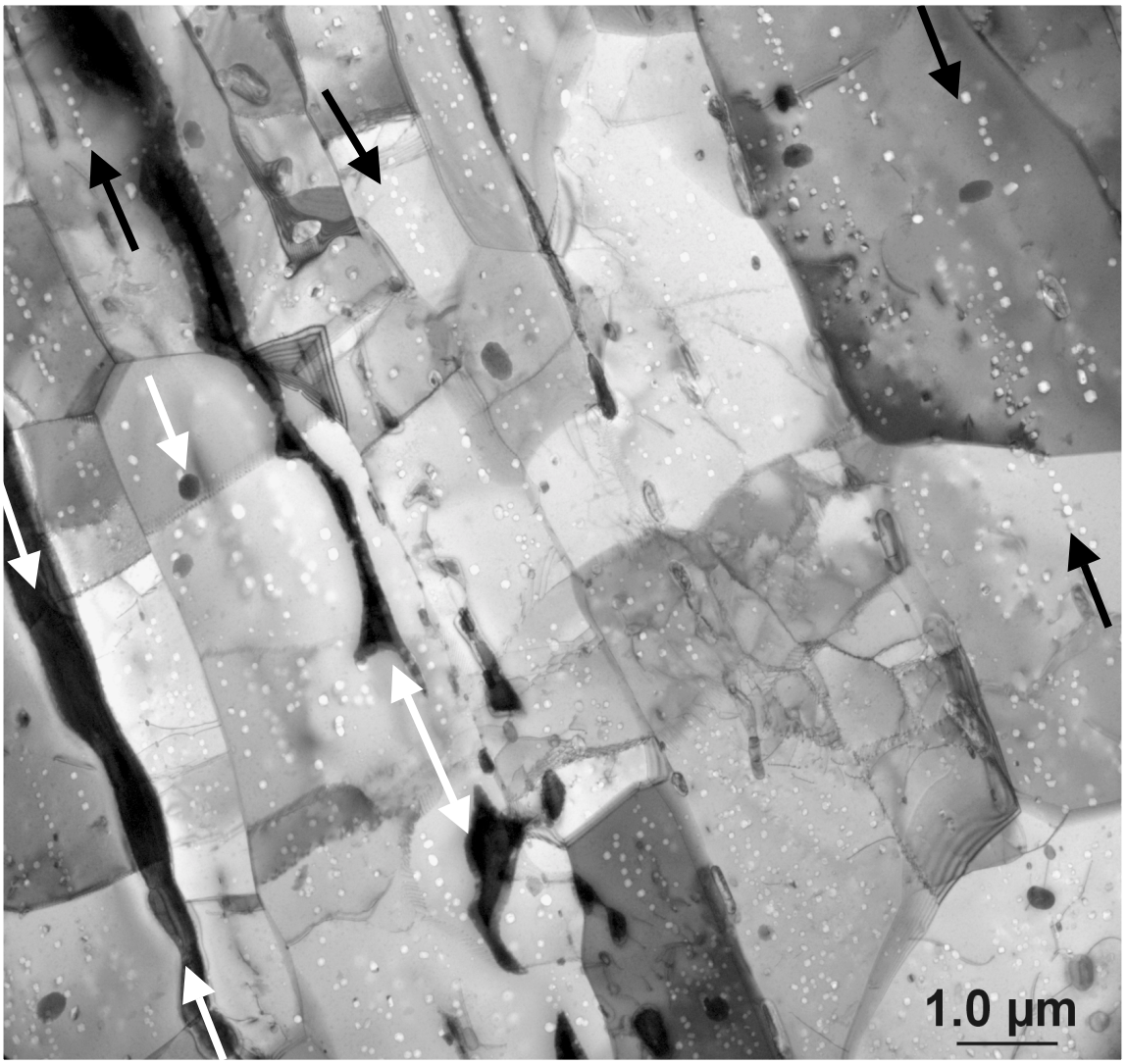

Figure 6.

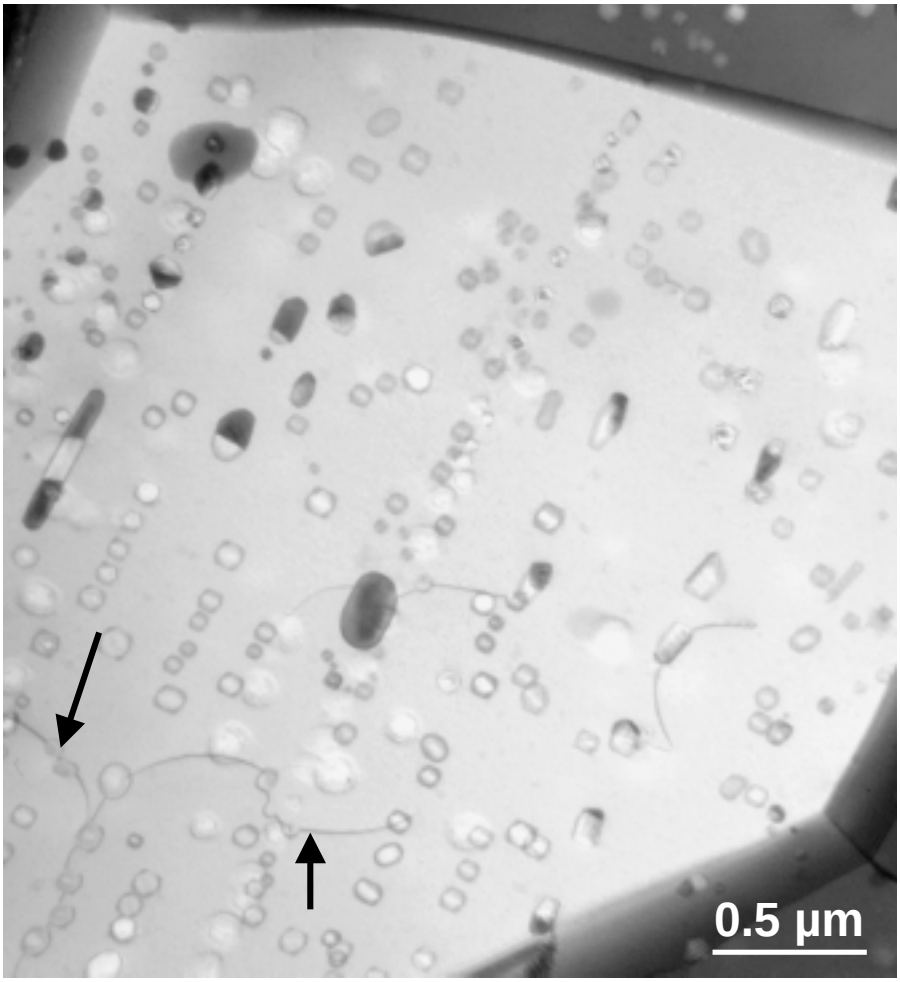

Figure 7

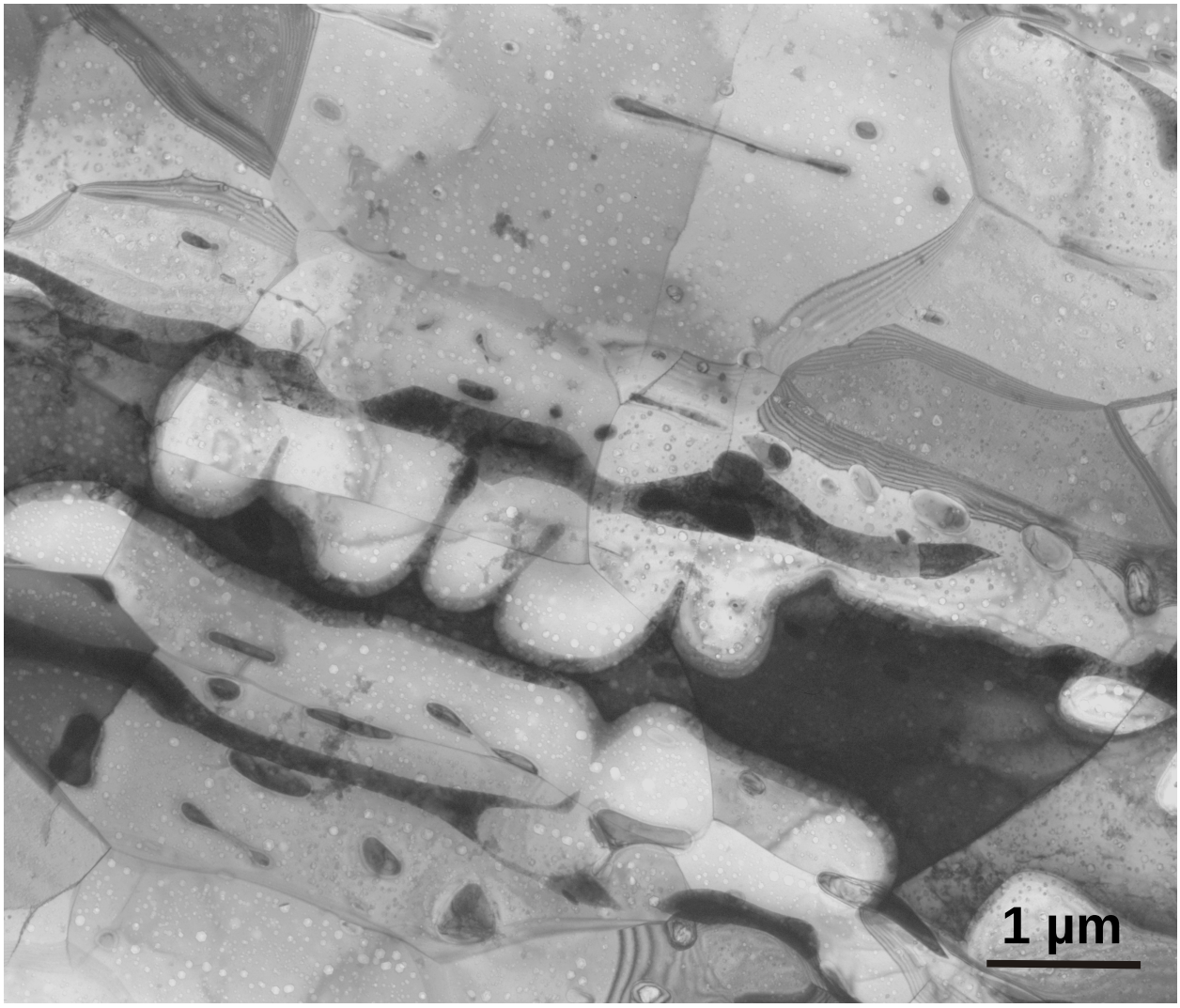

Figure 8

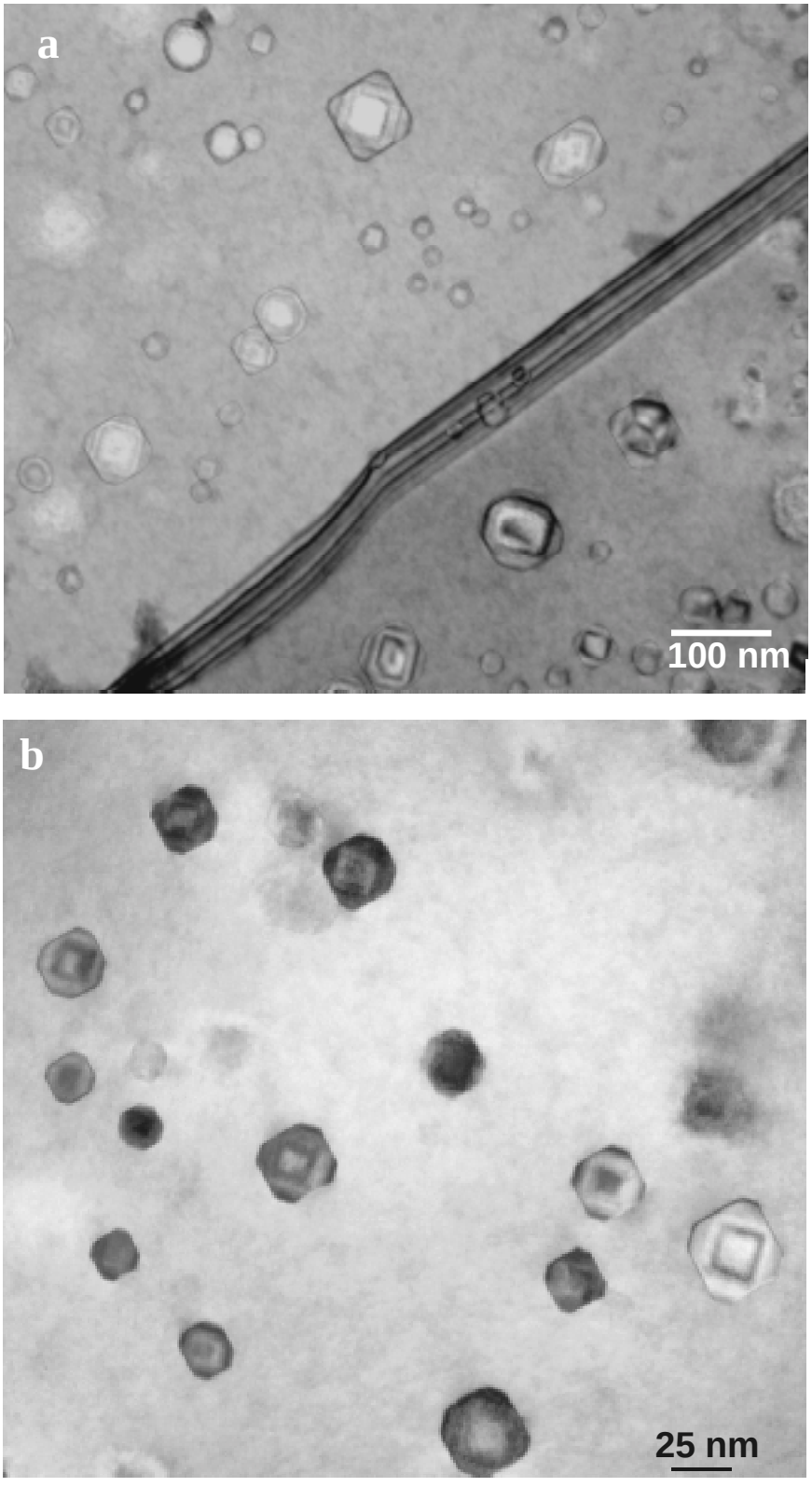

Figure 9

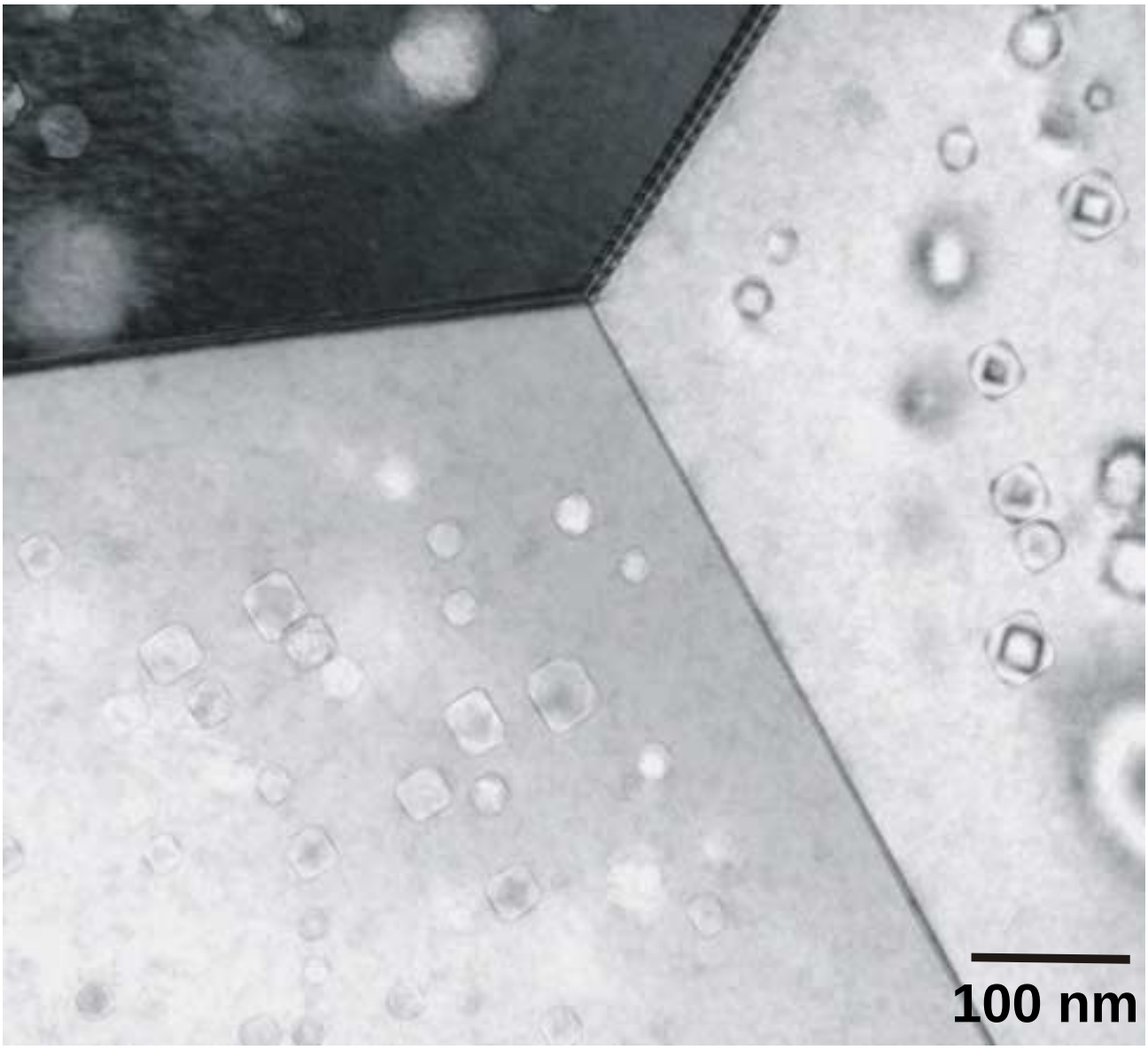

Figure 10